Evaluation of two processing routes for the synthesis of molybdenum oxide with cobalt addition

(Avaliação de duas rotas de processamento para produção de óxido de molibdênio com adição de cobalto)

C. P. B. Araujo[1]*, A. V. V. M. Frota[1], M. V. M. Souto[2], C. M. Barbosa[2], M. M. S. Silva[1], C. P. de Souza[1]

[1]Universidade Federal do Rio Grande do Norte, Chemical Engineering Department, Laboratório de Materiais Nanoestruturados e Reatores Catalíticos, 59078-970, Natal, RN, Brazil

[2]Universidade Federal do Rio Grande do Norte, Materials Science and Engineering Department, Natal, RN, Brazil

Abstract

Molybdenum oxides are very interesting technologic materials, which present several industrial uses. The addition of a second metal may enhance its catalytic properties as well as change electronic behavior. Several methodologies for adding a second metal can be found in the literature, however, the comparison between them is hardly ever found. Here two processing routes were tested for the synthesis of molybdenum oxide with cobalt addition: solid-state and wet routes. Ammonium molybdate and cobalt nitrate were used as starting materials and cobalt addition was carried out before calcination. Starting materials were characterized by SEM, FTIR, XRF, and XRD. Calcination products were evaluated by SEM, XRF, XRD and UV-vis spectroscopy. Calcined products whose doping was performed via solid-state presented smaller crystal size (~25 nm), larger cobalt retention (deviation, δ ~10%) and slightly smaller band gap in comparison to those doped via the wet route (~40 nm and δ>11%).

Keywords: molybdenum oxide, solid-state, wet impregnation, doping.

Resumo

Os óxidos de molibdênio são materiais tecnológicos muito interessantes, que apresentam diversos usos industriais. A adição de um segundo metal pode melhorar suas propriedades catalíticas, bem como alterar o comportamento eletrônico. Várias metodologias para adicionar um segundo metal podem ser encontradas na literatura, porém a comparação entre elas é dificilmente encontrada. Aqui duas rotas de processamento foram aplicadas para a síntese de óxido de molibdênio com adição de cobalto: via sólida e via úmida. Molibdato de amônio e nitrato de cobalto foram usados como materiais de partida e a adição de cobalto foi realizada antes da calcinação. Os materiais iniciais foram caracterizados por MEV, FTIR, FRX e DRX. Os produtos de calcinação foram avaliados por MEV, FRX, DRX e espectroscopia UV-vis. Produto calcinado cuja dopagem foi realizada via estado sólido apresentou menor tamanho de cristal (~25 nm), maior retenção de cobalto (desvio, δ ~10%) e band gap levemente menor em comparação com aquele dopado por via úmida (~40 nm e δ>11%).

***Palavras-chave**: óxido de molibdênio, estado sólido, impregnação a úmido, dopagem.*

INTRODUCTION

Metal molybdates are versatile and interesting materials that have applicability in various fields, such as in the production of sensors, capacitors, photocatalysts, and others [1]. These uses are mainly related to molybdenum oxidation states which can vary in a wide range [2]. Metal oxides can present several oxidation states, which make possible the occurrence of a great variety of redox processes over their surfaces [3]. This also indicates superior electrochemical storage capacity [4]. Metal oxides over support materials are, therefore, used as catalysts in a large variety of commercial processes that involve the conversion of hydrocarbons, such as hydrotreatment reactions [5]. Among metal oxides, molybdenum oxide, particularly, presents a set of properties which, in addition to its multiple oxidation states, may be interesting in electrochemical storage [6], heterogeneous catalysis [7], and photocatalysis [8]. Recently, much attention has been paid to the preparation and performance of mixed metal oxide catalysts, as the addition of a second metal to the oxide structure could change electronic and structural characteristics of the material, leading to superior final behavior in those areas. The second metal could act as a promoter of the catalytic performance due to the increased number of active sites or due to the greater availability of them for the reaction [9]. And, in comparison to monometallic compounds, mixed transition metal compounds present higher electrochemical activity, which can be attributed to their richer redox reactions and improved electronic conductivity [10].

Industrially used hydrodesulfurization catalysts, for example, have the Co-Mo system as the active phase for

**cpbaraujo@gmail.com*

https://orcid.org/0000-0002-9597-0434

the partial oxidation of hydrocarbons reactions and the cobalt addition is responsible for much of the gain in catalytic activity in comparison to pure molybdenum sulfide catalyst [5, 11, 12]. In general, these materials can be seen as the product of adding CoO or NiO to MoO_3 over Al_2O_3, or other support material, and composition lies in the range from 12 to 20 wt% of CoO in relation to MoO_3 [5]. Metal molybdates compounds have been synthesized by various methods such as precipitation [2, 13], sol-gel [14], solid-state [15], hydrothermal [10], etc. Most of them require high temperatures and harsh conditions, or elaborate and long chemical routes. In the solid-state reaction from the oxides, for example, temperatures in the range of 1000 °C can be found [15]. It is well-known that the synthesis method, starting materials, and reaction parameters play an important role in the physicochemical properties of nanomaterials, which can strongly influence the optical, electrical, and electrochemical properties. In the current study, two simple methodologies were tested for the synthesis of molybdenum oxide with cobalt addition and their effect over final products' properties was evaluated in terms of morphology, cobalt content retention, crystal size, and band gap.

EXPERIMENTAL

Ammonium molybdate [AM, $(NH_4)_2MoO_4$, Sigma Aldrich, 99%) and cobalt nitrate [$Co(NO_3)_2.6H_2O$, Cromato, 98%) were used as starting materials. Two doping routes were tested. The solid-state (SS) route consisted of the physical mixture of reactants in the desired compositional range (Co content of 3, 5 and 10%) in an agate mortar until complete visual uniformity. Wet route (WI) consisted of dissolving the two salts in water and letting the solution slowly evaporate under stirring at ~70 °C until a semi-dry mud was obtained. The mud was then transferred to an alumina crucible for further drying in a muffle furnace (EDG, Inox Line 3000) at 80 °C for 6 h to obtain a dry powder before calcination. All doped starting materials were characterized by X-ray diffraction (XRD, Bruker, D8 Advance, CuKα, 40 kV, 5 °/min, 40 mA) and Fourier-transform infrared (FTIR) spectroscopy (Bruker, Vetex 70). Scanning electron microscopy (SEM, FEI, Quanta-200FEG) was also performed on the powders with 5% Co.

Final oxides were produced by calcination of doped precursors. This consisted of heating them from room temperature to 500 °C (under a 5 °C/min heating rate) and keeping this condition for 180 min in the muffle furnace. The as-produced materials were characterized by X-ray fluorescence (XRF) spectroscopy (Shimadzu, EDX-720, air atmosphere), XRD, and SEM, and had their crystallite sizes estimated by the Scherrer method. UV-vis spectroscopy (Shimadzu, 2600) was also performed in order to calculate the band gaps of the doped oxides.

RESULTS AND DISCUSSION

Precursors' evaluation

XRD evaluation: in Fig. 1 the XRD pattern for the ammonium molybdate powder used in this study is presented. Two main crystal phases were observed: $(NH_4)_2Mo_2O_7$ (ICSD 4152) in a triclinic arrangement and $(NH_4)_2Mo_2O_4$ (ICSD 408750) which is monoclinic. In Fig. 1, the ten most intense peaks were labeled and the corresponding crystal phases are attributed. Table I presents the identified crystal phases for each doped material. In all of them, the same $(NH_4)_2Mo_2O_7$ phase was observed and in the lower compositional levels $(NH_4)_6Mo_7O_{24}.4H_2O$ was also obtained. At 3% Co addition, no changes in the obtained XRD pattern were seen upon comparing processing routes. However, at 5% Co addition, the processing route caused a difference in the obtained XRD patterns. For the material synthesized via solid-state route the two identified phases were $(NH_4)_2Mo_2O_7$ (ICSD 4152, triclinic) and $(NH_4)_6Mo_7O_{24}.4H_2O$ (ICSD 4153, monoclinic), while for the material produced via wet route, $(NH_4)_8Mo_{10}O_{24}$ (ICSD 4152, triclinic) was verified but not the hydrated phase. This can have occurred because in the wet route the solid underwent a drying step that was not present in the solid-state process. At this step, some water

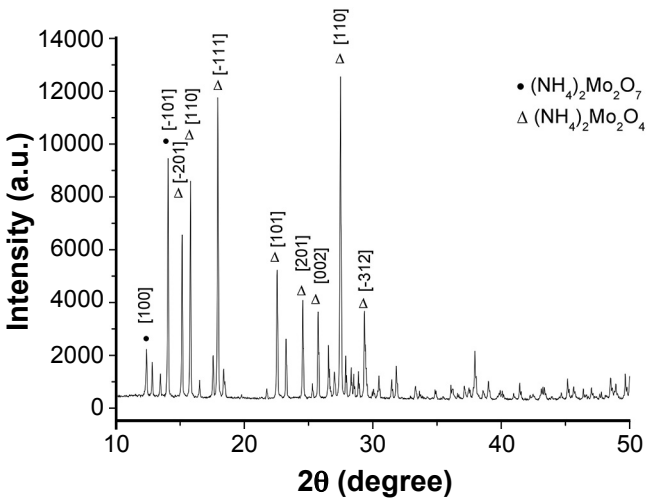

Figure 1: XRD pattern of the ammonium molybdate material used as Mo source.
[Figura 1: Padrão de difração de raios X do molibdato de amônio usado como fonte de Mo.]

Table I - Crystal phases identified in the doped precursors and pure ammonium molybdate (AM).
[Tabela I - Fases cristalinas identificadas nos precursores dopados e no molibdato de amônio (AM).]

Sample	AM	Solid-state			Wet route		
Co content (%)	0	3	5	10	3	5	10
$(NH_4)_2Mo_2O_4$ [a]	x						
$(NH_4)_2Mo_2O_7$ [b]	x	x	x	x	x	x	
$(NH_4)_6Mo_7O_{24}.4H_2O$ [c]		x	x		x		
$(NH_4)_8Mo_{10}O_{24}$ [b]						x	x
$Co(NH_3)_3(NO_2)_3$ [d]							x

[a] *ICSD 408750, monoclinic;* [b] *ICSD 4152, triclinic;* [c] *ICSD 4153, monoclinic;* [d] *triclinic.*

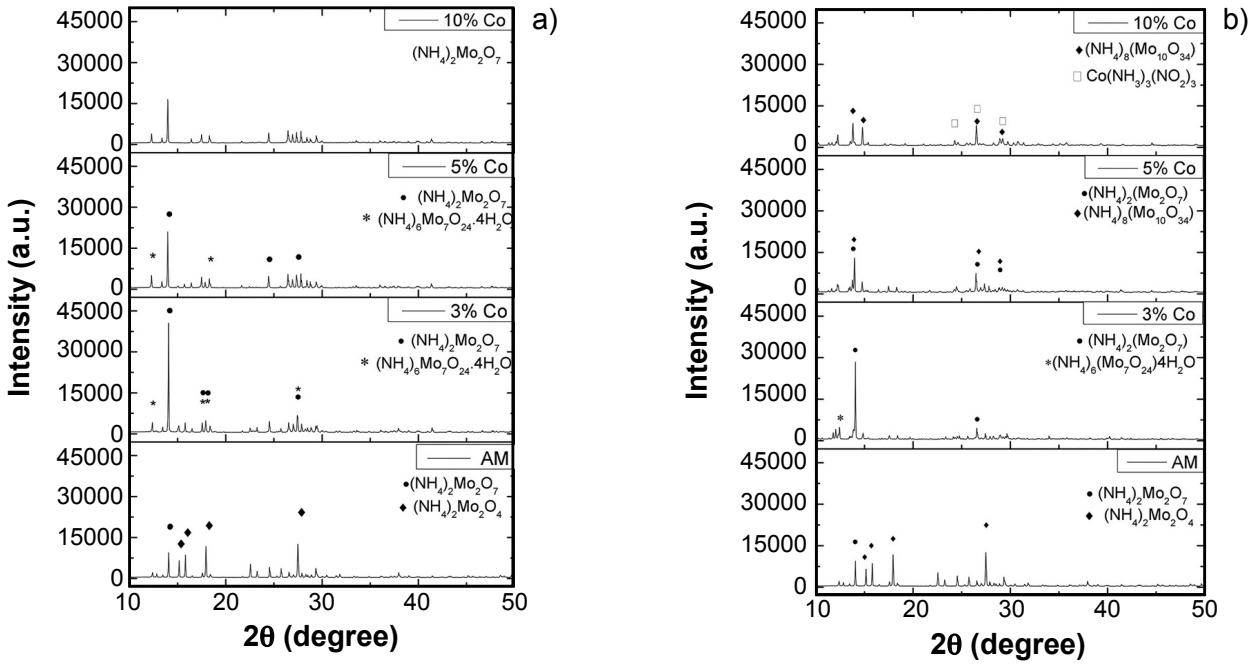

Figure 2: XRD patterns of AM and precursors doped via: a) solid-state; and b) wet route.
[Figura 2: Padrões de difração de raios X de AM e precursores dopados por: a) via sólida; e b) via úmida.]

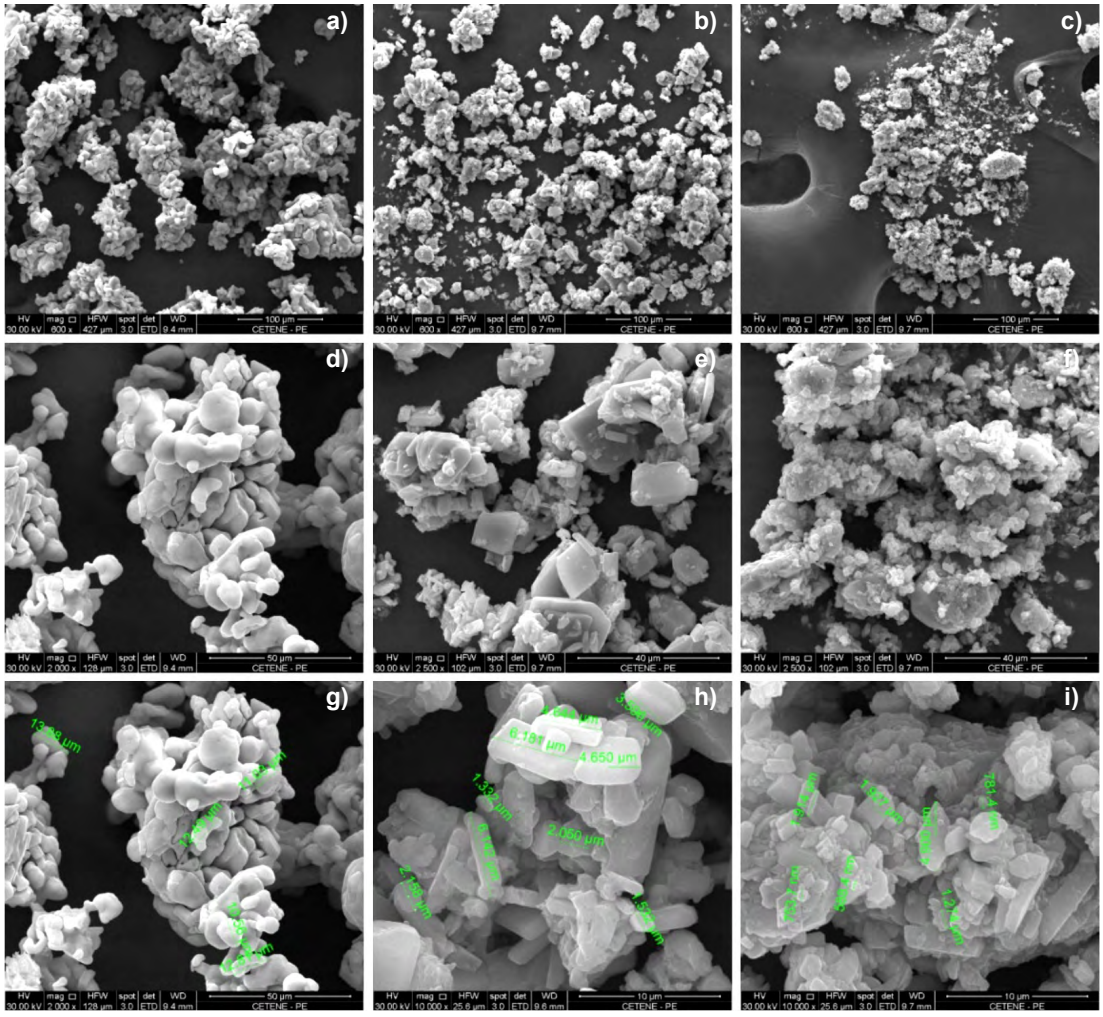

Figure 3: SEM images of AM (a,d,g) and precursors doped via solid-state (b,e,h) and wet route (c,f,i).
[Figura 3: Imagens de MEV do AM (a,d,g) e precursores dopados por via sólida (b,e,h) e via úmida (c,f,i).]

Table II - Crystallite sizes of the doped precursors and AM estimated by Scherrer's methodology.
[Tabela II - Tamanhos de cristalito estimados pela metodologia de Scherrer dos precursores dopados e AM.]

Sample	AM	Solid-state			Wet route		
Co (%)	0	3	5	10	3	5	10
Dp (nm)	139.2	117.4	129.1	121.7	116.9	99.1	93.7

elimination can occur, thus accounting for the different XRD patterns. In fact, other researchers [16] have found that this crystal phase can be produced by the heat treatment of $(NH_4)_6Mo_7O_{24}.4H_2O$ in mild temperatures for long periods. For the material with 10% Co produced via wet route, a second-phase containing cobalt was identified. This was not observed for the powder doped via the solid-state route at this compositional level. This indicated for the decreased insertion of Co ions in materials doped via wet route in comparison to solid-state doped ones.

Fig. 2 presents all raw XRD patterns with peak attribution for the doped precursors. In Fig. 2a the patterns of the materials doped via solid-state are shown and in Fig. 2b those of the materials doped via wet route. Diffraction peaks became more intense when cobalt was added, though the higher the Co content, the less pronounced this effect was. The increase in peak intensity of doped powders in comparison to pure AM was attributed to processing which improved the powders crystallinity. We considered this to be the cause of such behavior as all sampling and technical procedures for the analysis were carried out by well trained and experienced technicians, following strict analysis procedures, therefore all human effects were disregarded. For the solid-state methodology, this increase in powder crystallinity was considered to be due to the decrease in particle size caused by shear and compression during mixing, whereas on the wet impregnation route the powders were dissolved and recrystallized.

SEM: for a comparative morphological evaluation of the doping process SEM analysis was carried out on the materials with 5% Co addition and on pure AM. Fig. 3 presents the images for AM, solid-state (SS) doped and wet impregnation (WI) doped precursors. Images with three magnifications are presented for each powder. Comparing the samples at low magnification (Figs. 3a, 3b and 3c), one can observe the largest agglomerates produced via the WI route. SS doped precursor also seems to have larger agglomerates than the original AM powder. Several types of forces can play a role in the agglomeration of a given powder: van der Waals', magnetic, electrostatic and solid bridging forces. The importance of a given force over agglomeration depends on particular characteristics of the material. Van der Waals' forces are particularly significant when the particle size is less than 1 μm and increase as particle size decreases [17]. In Figs. 3g, 3h, and 3i, some particle size measurements of the doped precursors are presented. No apparent porosity was observed on the doped powders, and in all cases a platelet shape was attained after

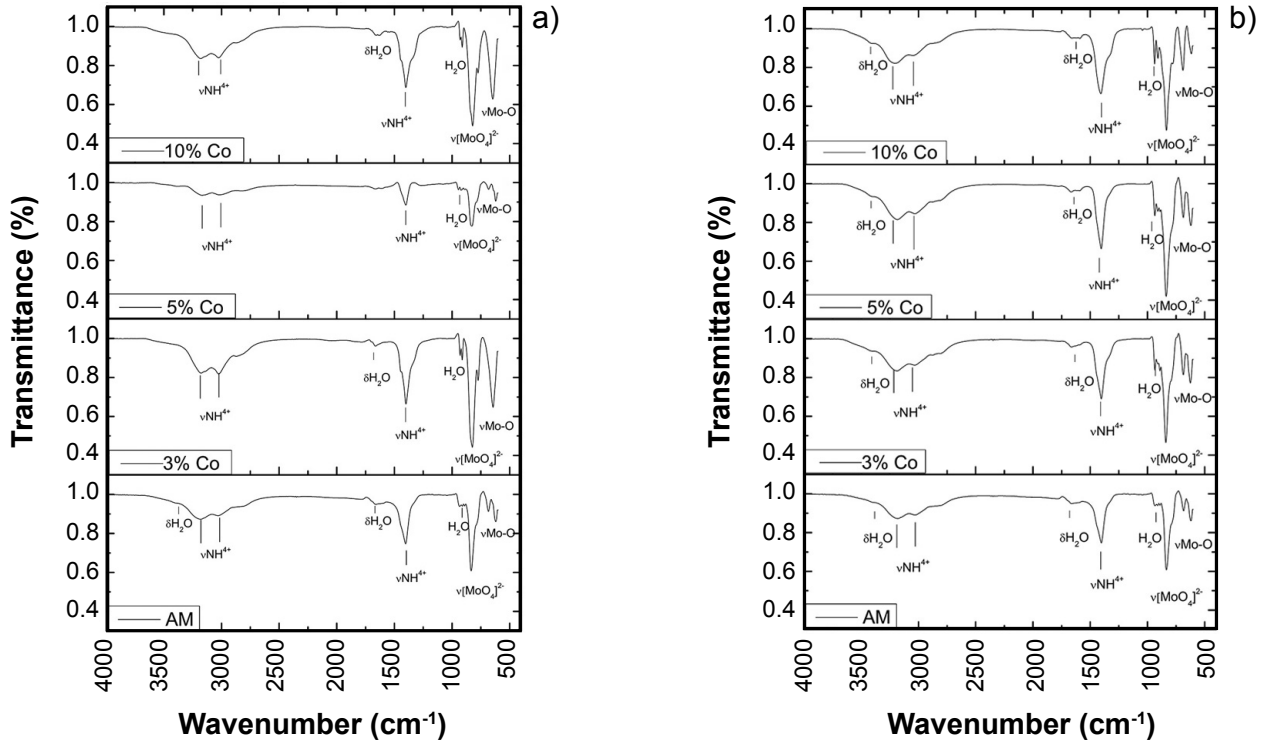

Figure 4: FTIR spectra of AM and precursors doped via: a) solid-state; and b) wet route.
[Figura 4: Espectros de FTIR de AM e precursores dopados por: a) via sólida; e b) via úmida.]

processing (Figs. 3e and 3f) which differed considerably from the rounded shape particles verified for the AM unprocessed powder (Fig. 3d).

Crystallite size: Table II presents estimated crystallite sizes for the doped precursors and for AM based on Scherrer's method. A slight tendency towards decreasing crystallite size with increasing Co content was noted. Precursors derived from WI methodology presented smaller crystallite sizes than their pairs doped via the solid-state route. These calculations were in accordance with XRD observation, where the material became more crystalline as cobalt was added and due to processing.

FTIR: chemical bonds' evaluation was performed on the basis of FTIR analysis for both pure AM and doped precursors. In Fig. 4a ammonium molybdate spectrum is presented and the product of its doping via solid-state route is shown for comparison and in Fig. 4b the same is presented for those doped via wet impregnation. All identified chemical bonds are indicated. While no clear relation between cobalt content and the obtained spectra was seen, there was evidence of the effect of the doping route on the chemical bonds of the powders. It was observed in the powders produced via the solid-state route the presence of a metallic bond (wavenumber close to 600 cm^{-1}). This was attributed to Mo-O stretching. This bond was not present in the spectra of the wet doped materials with the same intensity. It was assumed that the intensification of the Mo-O stretching can be due to the accommodation of the crystal structure caused by the cobalt insertion. Even though no chemical bonds regarding the presence of cobalt ions were observed, this did not attest for the absence of them, as the responses of metal-metal bonds occur at low wavenumbers in the range that the available equipment could not perform a proper analysis.

Oxides' assessment

XRD: the crystal phase formation was assessed via XRD of the calcined powders. Fig. 5 presents the raw data provided by XRD with peak identification. Pure MoO_3 with orthorhombic structure (ICSD 76365) and $CoMoO_4$ with monoclinic structure (ICSD 23808) were obtained in all cases. In Fig. 5a, solid-state doped oxides' patterns are presented. A tendency for decreasing peak intensities with increasing doping content can be observed. In Fig. 5b, wet impregnation derived oxides' patterns are presented, and the same can also be seen. This decreased peak intensity upon Co addition indicated smaller crystal sizes of the doped oxides in comparison to pure molybdenum oxide powder. Processing had no effect on crystal structure or phase formation as far as could be evaluated. Peak intensities for the $CoMoO_4$ phase were more pronounced for oxides derived from wet impregnation route, whereas for solid-state doped ones their relative intensities were remarkably lower in comparison to MoO_3. As Co ions are expected to be in both identified structures (in MoO_3 as structural defects or forming $CoMoO_4$), lower relative intensities can be related to a larger amount of Co being present in the MoO_3 phase. That can be interesting for catalytic purposes as there can be a more intrinsic synergistic effect of Co ions.

Crystallite size: estimates were performed on the mathematical profile produced by fitting the raw XRD data with the patterns presented in the previous sections. Scherrer (Eq. A), Williamson-Hall (Eq. B), and Halder-Wagner-Langford (HWL, Eq. C) equations were tested for all materials. Though the Scherrer method is simpler than others, it served for the purpose of an estimation of the actual crystallite size as it does not consider any kind of anisotropic effect on the material. This parameter was

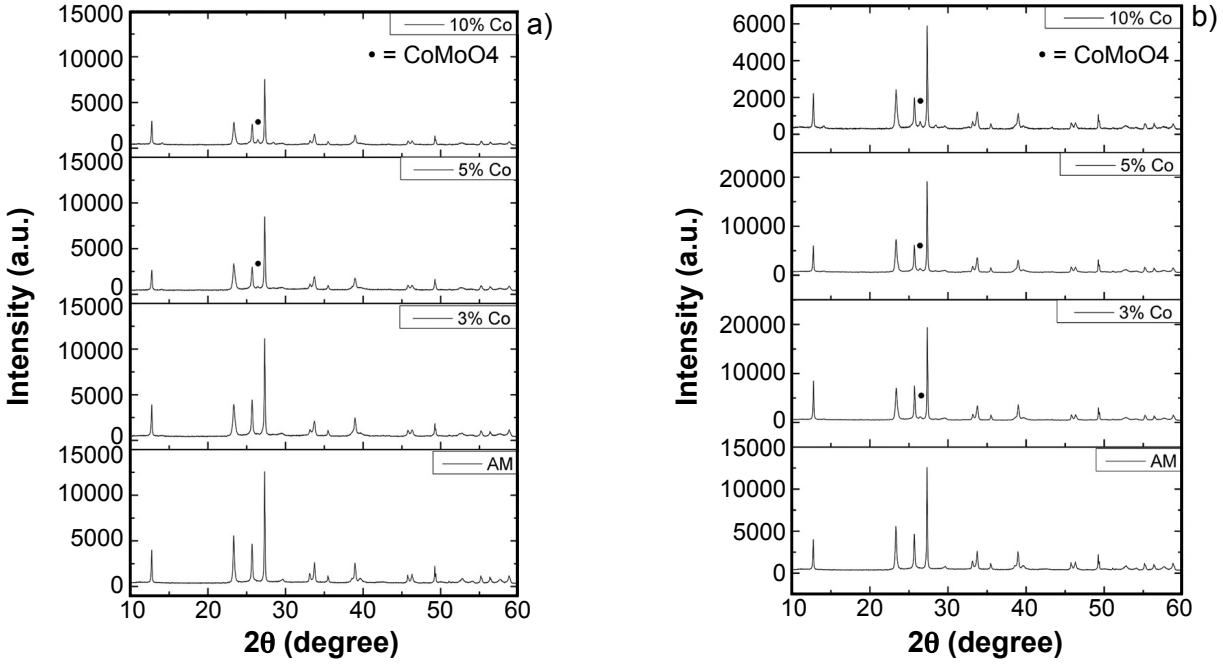

Figure 5: XRD patterns for oxides doped via: a) solid-state; and b) wet route.
[Figura 5: Padrões de difração de raios X dos óxidos dopados por: a) via sólida; e b) via úmida.*]*

accounted on HWL and Williamson-Hall methods, which also allowed microstrain (ε) estimation of the crystallite. All calculations were performed using FWHM (full width at half maximum) data of each peak on the XRD patterns.

$$D = \frac{k.\lambda}{\beta.\cos\theta} \quad (A)$$

$$\frac{\beta.\cos\theta}{\lambda} = \frac{k}{D} + 4.\varepsilon.\frac{\sin\theta}{\lambda} \quad (B)$$

$$\left(\frac{\beta.\cos\theta}{2.\sin\theta}\right)^2 = \frac{1}{D}\cdot\frac{\beta.\cos\theta}{(2.\sin\theta)^2} + \left(\frac{\varepsilon}{2}\right)^2 \quad (C)$$

Table III presents crystallite size estimates of the produced oxides. Correlation coefficients for calculations using HWL and Williamson-Hall methods were quite low in all cases, which indicated that anisotropy effects can be considered negligible. Therefore, Scherrer's estimates were considered adequate for analyzing the crystallite sizes. Comparing the effect of processing route on the crystal sizes of the produced oxides with the same Co content, one can verify that solid-state doped oxides presented remarkably smaller crystal sizes than those derived from the wet route. This can be directly related to energy considerations regarding the processing conditions: during wet route syntheses, the salts were dissolved in water and recrystallized, and then subject to drying in muffle furnace before calcination. The latter step was not present in solid-state route and can have induced crystal growth as more energy was provided to them by the heating process thus forming larger final products when subject to calcination. This was in agreement with nucleation and growth theory proposed by Avrami [18]. Evaluating the effect of the Co addition, one can see that for solid-state methodology there seems to be a tendency of increasing crystal size with increasing Co content.

XRF: compositional evaluation was performed on the basis of XRF analysis (Table IV). Powders produced via wet impregnation presented greater compositional deviation (δ>10%) from the intended cobalt content, than the oxides produced from the solid-state mixing process (δ~10%). This can be attributed to the stirring step as cobalt nitrate started to decompose at temperatures as low as 80 °C, and water started to evaporate from the mixture, causing some of the solid material to attach itself and on the walls of the beaker. In addition, this process had more mass transferring steps (from beaker to crucibles and sample holders) than solid-state mixing route, which could also be responsible for the larger deviation, though experimental care was taken and all experiments were performed thrice.

Table IV - XRF compositional evaluation (molar%) of the doped oxides.
[Tabela IV - Avaliação composicional (% molar) dos óxidos dopados por FRX.]

Co content	Solid-state			Wet route		
Theoretical	3	5	10	3	5	10
XRF verified	2.91	4.59	8.77	2.63	4.06	6.44
Deviation δ	2.9	8.1	12.4	11.8	18.8	35.6

UV-vis spectroscopy: band gap evaluation was performed on the produced oxides in order to analyze its applicability as a medium for electrochemical catalysis [19]. The data are presented in Table V. Fig. 6 shows a typical determination of the band gap from the extrapolation of the linear part of the Kubelka-Munk function [F(R), Eq. D] as a function of the photon energy (hν). Eq. E relates the photon energy to the absorbance of the material which is, in turn, obtained through UV-vis analysis:

$$F(R) = \alpha = \frac{(1-R)^2}{2.R} \quad (D)$$

$$\alpha.h\nu = k.\,(h\nu - E_{gap})^n \quad (E)$$

Table V - Band gap data of molybdenum oxide and doped oxides.
[Tabela V - Valores de band gap dos óxidos dopados e puro.]

	MoO_3	SS		WI	
Co (%)	0	5	10	5	10
E_{gap} (eV)	3.34	3.35	3.33	3.37	3.35

Table III - Crystallite size estimates of the produced oxides based on Scherrer, Williamson-Hall, and HWL methods.
[Tabela III - Tamanhos de cristalito dos óxidos estimados pelas metodologias de Scherrer, Williamson-Hall e HWL.]

Synthesis method	Co (%)	HWL			Scherrer	Williamson-Hall		
		d_{HWL} (nm)	ε_{HWL}	R^2	d_{Sch} (nm)	d_{WH} (nm)	ε_{WH}	R^2
Wet route	3	0.13	0.35	0.04	79.91	37.61	0.001	0.042
	5	0.02	0.31	0.24	80.24	39.72	0.000	0.002
	10	0.94	0.36	0.00	47.37	28.27	0.001	0.011
Solid-state	3	0.03	0.12	0.19	41.68	49.84	0.001	0.107
	5	0.28	0.46	0.02	41.82	49.74	0.003	0.032
	10	0.29	0.47	0.01	44.60	44.24	0.001	0.051
MoO_3	-	0.13	0.05	0.09	78.43	122.6	0.001	0.042

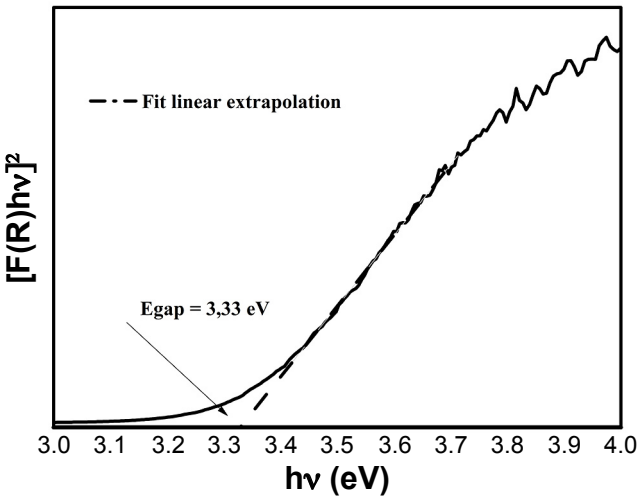

Figure 6: Linear extrapolation of the Kubelka-Munk function for band gap estimate.
[Figura 6: Extrapolação linear da função Kubelka-Munk para estimativa do band gap.]

where k is the absorption constant, which is dependent on the material, and n can assume values of 1/2, 3/2, 2 and 3 according to the electronic transition (directly allowed, indirectly allowed, directly prohibited or indirectly prohibited, respectively) that occurs; n was taken to be ½ according to [20]. Direct transition is often used to describe crystalline MoO_3 films, with reported optical band gaps in the range of 2.8 to 3.5 eV [21, 22]. No significant changes in the band gap of the materials could be observed regarding the change in methodology. In general, solid-state (SS) doped powders presented a slightly smaller band gap than wet impregnated (WI) derived materials. Comparing with the pure molybdenum trioxide (~3.34 eV), most doped materials presented slightly larger gaps. These data are in agreement with the band gap evaluation performed on MoO_3 films in [23], where 3.2 eV gap was observed. Even though the presence of the second metal promoted an increase in the band gap, its presence is of importance in other aspects of electrochemical catalysts, such as the presence of a greater

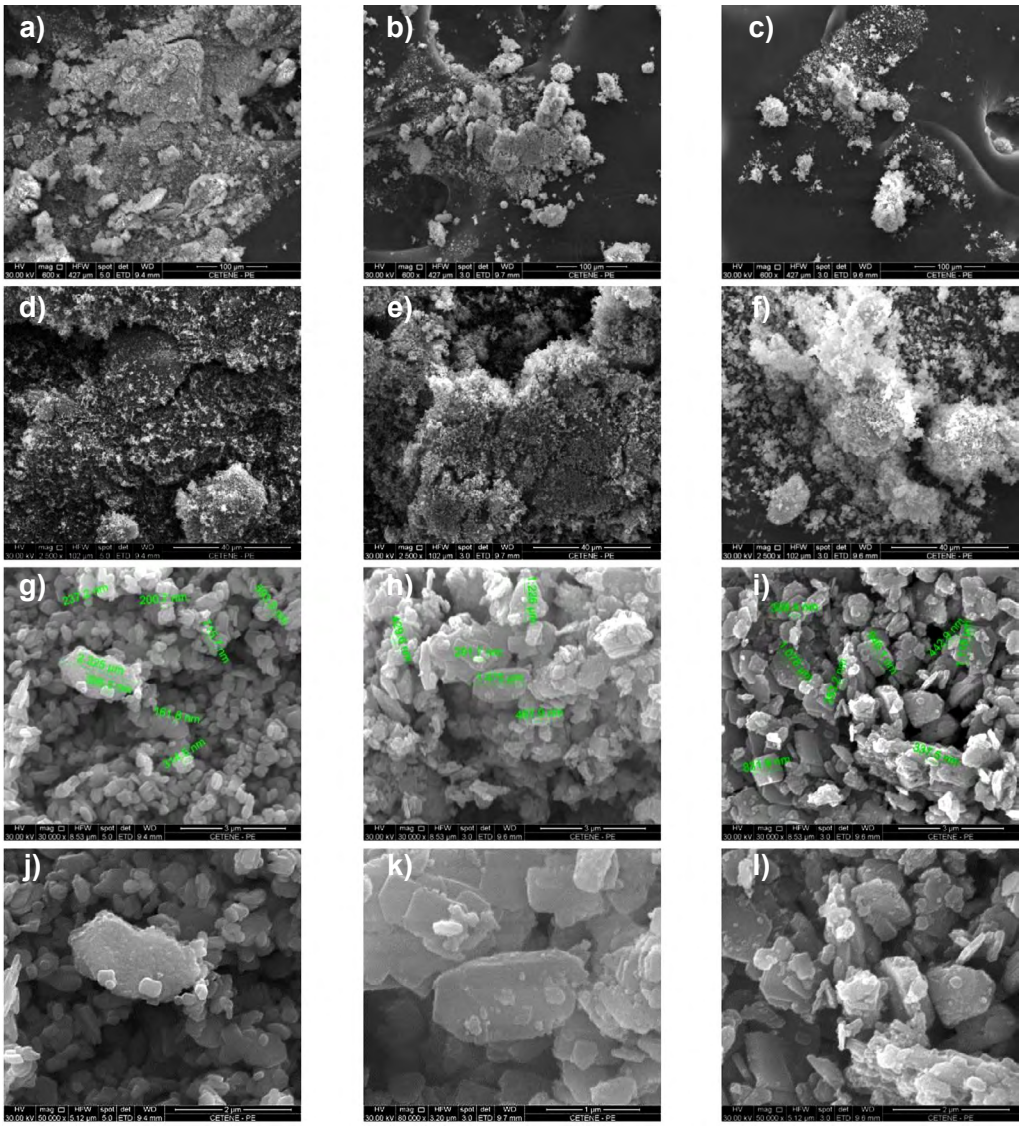

Figure 7: SEM images of MoO_3 (a,d,g,j) and oxides doped via solid-state (b,e,h,k) and wet route (c,f,i,l).
[Figura 7: Imagens de MEV do MoO_3 (a,d,g,j) e óxidos dopados por via sólida (b,e,h,k) e via úmida (c,f,i,l).]

amount of catalytic sites and chemical promotion of the reaction.

SEM: morphological evaluation was also performed on the produced oxides. Fig. 7 presents SEM micrographs for pure MoO_3 (Figs. 7a, 7d, 7g, and 7j) produced from AM calcination, and the 5% Co-doped oxides derived from solid-state mixture of powders (Figs. 7b, 7e, 7h, and 7k) and wet impregnation (Figs. 7c, 7f, 7i, and 7l). Pure and doped oxides presented no apparent porosity. A terraced platelet shape with well-defined corners was observed. This platelet shape is characteristic of the major MoO_3 phase [24] identified by XRD analysis. This can be observed in Figs. 7j to 7l, where one can see that processing seems to have made it more pronounced for doped oxides. It was also noteworthy the fact that these particles seemed to be arranged in layers of platelets, thus forming what could be seen as a lamellar structure that can easily pack to form agglomerates (Figs. 7d to 7f). Comparing agglomerates of particles, one can see that the powder produced by solid-state doping tended to form larger agglomerates in comparison to wet route derived oxides. This can be seen on micrographs of low magnification (Figs. 7a to 7c), but also at high magnification (Figs. 7g to 7i), where individual particles were measured; Table VI summarizes the average values of measured particle size.

Table VI - Particle size (nm) estimates from SEM images of MoO_3 and oxides doped via solid-state (SS) and wet route (WI).
[Tabela VI - Tamanhos de partícula (nm) do MoO_3 e óxidos dopados por via sólida (SS) e úmida (WI) estimados pelas imagens de MEV.]

MoO_3	SS	WI
615	778	677

CONCLUSIONS

It was observed that the oxides derived from solid-state (SS) mixing were able to retain the second metal (cobalt) more and better than those derived from wet impregnation (WI). These materials (SS) presented smaller crystallite sizes than those produced via the WI route (~40 nm in comparison to ~80 nm, respectively). Besides, they presented in the XRD patterns lower relative intensities of $CoMoO_4$ phase, which was considered as one of the parameters to indicate the presence of Co in the MoO_3 structure, and band gaps slightly smaller (~3.34 eV in comparison to ~3.37 eV). This set of advantageous characteristics indicated that the use of a simple methodology of manually mixing salts containing the final species could be used for synthesizing MoO_3 with Co addition with more interesting final properties than wet impregnation. Therefore, solid-state methodology was considered a more consistent route to produce these materials, with the advantage of simple scaling-up by the use of ball mills to promote the adequate mixing of starting materials.

ACKNOWLEDGMENTS

We specially thank the financial support by Fundação de Amparo à Ciência e Tecnologia de Pernambuco (FACEPE), Centro de Tecnologias Estratégicas do Nordeste (CETENE), Coordenação de Aperfeiçoamento de Pessoal de Nível Superior (CAPES), and Conselho Nacional de Desenvolvimento Científico e Tecnológico (CNPq) to help us develop this research.

REFERENCES

[1] G. Kianpour, M. Salavati-Niasari, H. Emadi, Superlattices Microstruct. **58** (2013) 120.
[2] M.C. Liu, L. Bin Kong, C. Lu, X.M. Li, Y.C. Luo, L. Kang, Mater. Lett. **94** (2013) 197.
[3] P. Buchel, K.H. Moretto, H.H. Woditsch, *Industrial inorganic chemistry*, 2nd ed., Wiley-VCH (2000).
[4] Y. Ma, G. Guan, C. Shi, A. Zhu, X. Hao, Z. Wang, A. Abudula, Int. J. Hydrogen Energy **39** (2014) 258.
[5] S. Matar, M.J. Mirbach, H.A. Tayim, *Catalysis in petrochemical processes*, Kluwer Acad. Publ. (1989).
[6] B. Bartlett, C. Soto, R. Wu, W.T. Tysoe, Catal. Lett. **21** (1993) 1.
[7] K.V.Chary, K.R.Reddy, G.Kishan, J.W.Niemantsverdriet, G. Mestl, J. Catal. **226** (2004) 283.
[8] L.T.C. Beltrame, "Caracterização de efluente têxtil e proposta de tratamento", M.Sc. Thesis, Un. Fed. Rio Grande Norte, Natal (2009).
[9] V.H.J. De Beer, J.C. Duchet, R. Prins, J. Catal. **72** (1981) 369.
[10] H. Chen, S. Chen, Y. Zhu, C. Li, M. Fan, D. Chen, G. Tian, K. Shu, Electrochim. Acta. **190** (2016) 57.
[11] E. Furimsky, in Catalysts for upgrading heavy petroleum feeds, Elsevier (2007).
[12] A. Sem, P. Pramanik, Mater. Lett. **50** (2001) 287.
[13] M. Edrissi, S. Samadanian-Isfahani, M. Soleymani, Powder Technol. **249** (2013) 378.
[14] E.A. Trusova, K.V. Kotsareva, E.V. Shelekhov, S.V. Kutsev, Nanotechnol. Russia **9** (2014) 325.
[15] J. Haber, A. Sosnowska, J. Ziółkowski, J. Solid State Chem. **16** (1976) 83.
[16] T. Konya, T. Katou, T. Murayama, S. Ishikawa, M. Sadakane, D. Buttrey, W. Ueda, Catal. Sci. Technol. **3** (2013) 380.
[17] P.A. Hartley, G.D. Parfitt, L.B. Pollack, Powder Technol. **42** (1985) 35.
[18] M. Avrami, J. Chem. Phys. **7** (1939) 1103.
[19] C. Ehrhardt, M. Gjikaj, W. Brockner, Thermochim. Acta **432** (2005) 36.
[20] M.S. Sena, M.M.S. Silva, A.G. Santos, A.L. Lopes-Moriyama, C.P. Souza, Mater. Res. **20** (2017) 485.
[21] M.M.S. Silva, M.S. Sena, A.L. Lopes-Moriyama, C.P. Souza, A.G. Santos, Ceram. Int. **44** (2018) 16606.
[22] K. Inzani, M. Nematollahi, F. Vullum-Bruer, T. Grande, T.W. Reenaas, S.M. Selbach, Phys. Chem. Chem. Phys. **19** (2017) 9232.

[23] V. Nirupama, M. Chandrasekhar, P. Radhika, B. Sreedhar, S. Uthanna, J. Optoelectron. Adv. Mater. **11** (2009) 320.

[24] V.M. Dieterle, "*In situ* resonance Raman studies of molybdenum oxide based selective oxidation catalysts", Doct. Thesis, Techn. Un. Berlin (2001).

(Rec. 18/03/2019, Rev. 27/06/2019, Ac. 10/08/2019)